Wave Motion 134 (2025) 103482

Contents lists available at ScienceDirect

Wave Motion

journal homepage: www.elsevier.com/locate/wamot

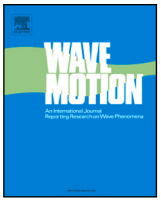

Evolution of nonlinear waves with heterogeneous damping and forcing

Ben S. Humphries *, Jack S. Keeler, Alberto Alberello, Emilian I. Părău

School of Engineering, Mathematics & Physics, University of East Anglia, Norwich, NR4 7TJ, UK

ARTICLE INFO

Keywords:
Nonlinear waves
Nonlinear Schrödinger equation
Dysthe equation
Damping
Forcing

ABSTRACT

Slowly modulated nonlinear-waves are ubiquitous in nature and their weakly nonlinear dynamics are described by the nonlinear Schrödinger equation (NLS) or its higher order version, i.e. Dysthe's equation. There is no inherent dissipation mechanism in these equations, however, in many physical systems the wave evolution is affected by energy gains and losses and therefore these NLS-like equations have to be modified to include these effects. Here, we focus on the evolution of wind-forced ocean waves propagating in ice-covered waters, such as in the polar regions. The peculiar feature of this physical system is the heterogeneous, frequency-dependent, attenuation. Here, we showcase the combined effect of higher order nonlinearity and heterogeneous dissipation on the wave dynamics.

1. Introduction

The propagation of nonlinear dispersive waves is an ubiquitous process in a range of physical systems: optics [1–4], quantum dynamics [5–7], ocean dynamics [8] and metamaterials [9]. The nonlinear dynamics generate solitary waves in optics and oceanography [10,11], and quantum memory effects in open quantum systems [12,13]. Accurate modelling of the dynamics of these systems is imperative for improving/developing interferometric devices [14], resonance energy transfer mechanisms and photosynthetic materials [15], as well as predicting rogue waves in the ocean [10,16]. In all these systems, the nonlinear Schrödinger equation (NLS) models the slow modulation of weakly nonlinear, dispersive, wave packets [17–19].

For ocean waves, the NLS is an evolution equation for the complex wave envelope (a) and the nonlinearity is expressed in terms of the wave steepness [$\epsilon = k_0 a$; where k_0 is the characteristic wavenumber, see for example 20]. The NLS is suitable for narrow-banded wave spectra and for low nonlinearity [18]. However, as the nonlinearity increases, higher order corrections in wave steepness must be introduced to overcome the narrow-banded assumption and better reproduce asymmetric wave spectra [21]. This set of equations is known as the Dysthe equation and hereafter is referred to as the "Higher Order Nonlinear Schrödinger equation" [HONLS; 21].

Forcing and damping are introduced in NLS-like models to reproduce a broader range of physical processes. In the context of ocean waves, loss is often associated with viscous-like attenuation at the interface [22–24] and gain with wind input [25–27]. Homogeneous forcing and damping have also been introduced in the framework of the HONLS [18,28–30].

Forcing and damping are due to different mechanisms, but both are linear operators and are commonly assumed to be constant across the wave spectrum. The resulting effect is a net loss/gain [25]. However, in many physical systems the attenuation rate is heterogeneous across the energy spectrum and depends on wave frequency. For example, waves propagating in sea ice are modelled by frequency dependent, heterogeneous, dissipation [31]. High frequency components undergo stronger attenuation, and the rate varies according to a power law in wave frequency with an exponent found to be between 2–5 [32–35]. Heterogeneous, frequency

* Corresponding author.
E-mail address: b.humphries@uea.ac.uk (B.S. Humphries).

https://doi.org/10.1016/j.wavemoti.2024.103482
Received 29 August 2024; Received in revised form 14 November 2024; Accepted 14 December 2024
Available online 3 January 2025

dependent, sea ice attenuation in the marginal ice zone has been recently introduced in the NLS by Alberello and Părău [36]. Alberello et al. [37] investigated the dynamics of an unstable wave train subjected to sideband perturbations, i.e. the modulational instability (MI) in presence of heterogeneous dissipation, while Alberello and Părău [36] and Slunyaev and Stepanyants [38] focused on the evolution of a broad-banded spectrum in sea ice, with Slunyaev and Stepanyants [39] including inertial sea ice properties that would better replicate ice sheets. Compared to an equivalent homogeneous attenuation, the heterogeneous dissipation significantly alters the wave dynamics. Similar results have been observed by Stuhlmeier et al. [40] for MI but in the framework of the spatial Zakharov equation. One of the striking features of heterogeneous damping is that it induces asymmetry in the wave spectrum, which would be better modelled in the framework of the HONLS.

Here, we introduce heterogeneous (frequency dependent) attenuation in the Dysthe equation in order to model frequency dependent ocean waves with broad-banded spectra. We will highlight the difference in the dynamics between the NLS and HONLS for varying degrees of nonlinearity and forcing/damping strength. In particular, we will show that only the HONLS captures the varying drift of the wave envelope.

2. Methodology

2.1. Model equations

We focus on the evolution of ocean waves in deep water propagating through sea ice in the marginal ice zone, in which the effect of inertia of the ice cover can be excluded (ice floes are small) and only viscous-like attenuation is therefore considered, and under the action of wind forcing. We therefore use the spatial version of the NLS and HONLS [41]. For ease of analysis we employ a coordinate system moving with the group velocity, and in this framework the Dysthe equation (HONLS) reads:

$$\underbrace{\frac{\partial a}{\partial x}+\frac{\mathrm{i}k_0}{\omega_0^2}\frac{\partial^2 a}{\partial t^2}+\mathrm{i}k_0^3 a|a|^2}_{\text{NLS}}=\Bigg(\underbrace{\Gamma}_{\text{Forcing}}-\underbrace{D}_{\text{Damping}}\Bigg)a+$$
$$\underbrace{\epsilon\frac{k_0^3}{\omega_0}\left(6|a|^2\frac{\partial a}{\partial t}+2a\frac{\partial|a|^2}{\partial t}+2\mathrm{i}a\mathcal{H}\left[\frac{\partial|a|^2}{\partial t}\right]\right)}_{\text{HO correction}}+$$
$$\epsilon\Bigg(\underbrace{\frac{4\mathrm{i}}{\omega_0}\Gamma}_{\text{HO Forcing}}-\underbrace{\frac{3\mathrm{i}}{\omega_0}D}_{\text{HO Damping}}\Bigg)\frac{\partial a}{\partial t}, \tag{1}$$

where $a(x,t)$ is the complex wave amplitude evolving along the slow spatial coordinate x, t the slow time, i the imaginary unit, and k_0 the wavenumber of the carrier wave (ω_0 is the angular frequency obtained from the dispersion relation $\omega_0=\sqrt{gk_0}$ where g is the gravitational acceleration). The forcing and damping terms are denoted by the operators Γ and D respectively and the Hilbert transform by $\mathcal{H}[\{\cdot\}]$ where $\mathcal{F}\left[\mathcal{H}[\{\cdot\}]\right]=-\mathrm{i}\cdot\mathrm{sgn}(\omega)\mathcal{F}[\{\cdot\}]$, and $\mathcal{F}$ and $\mathcal{F}^{-1}$ denote forward and backward Fourier transforms in t. The corresponding NLS is obtained by suppressing all higher order (HO) terms, i.e. setting $\epsilon=0$.

The peculiarity of the equation is that, to achieve heterogeneous attenuation, D is defined in Fourier space as [37]:

$$D[a(x,t)]=\mathcal{F}^{-1}\left[D(\omega)\mathcal{F}[a]\right],\qquad D(\omega)=\alpha_n\omega^n,\qquad \alpha_n\in\mathbb{R}, \tag{2}$$

Higher order forcing/damping are obtained from a linear expansion in ω_0 [18]. It is worth noting that if n is a positive integer (as it will be in this article), the operator D is simply:

$$D[a(x,t)]=(-\mathrm{i})^n\alpha_n\frac{\partial^n}{\partial t^n}a(x,t). \tag{3}$$

2.2. Experimental conditions

Two suites of numerical experiments are considered. In the first set we vary the nonlinearity, and in the second the forcing/damping strength is varied while maintaining a fixed ratio. Numerical experiments are run for both constant and heterogeneous damping, and for both the NLS and HONLS model. These simulations are compared against a benchmark model in which both the forcing and damping have been set to zero.

For the heterogeneous damping we assume $n=3$ [37], so the frequency dependent dissipation is $D(\omega)=\alpha_3\omega^3$. When the damping is homogeneous the rate of dissipation of the carrier is used, i.e $D(\omega)=\alpha_3\omega_0^3$. The choice of $n=3$ is supported by theoretical studies and their agreement with experimental measurements [31]. When n is odd we do not expect qualitative differences in dynamics. When present, the forcing, Γ, is homogeneous, i.e. constant across the frequency range, and is set to balance $D(\omega_0)$ such that the two are in equilibrium. The choice of α_3 is made to achieve weak dissipation ($\approx 5\%$ of the energy over 100 wavelength) to explore a dynamical regime in which nonlinearity remains relevant. Stronger attenuation would completely suppress the interesting nonlinear dynamics as shown in Alberello et al. [37].

All experiments are conducted for $k_0 = 10\ \mathrm{m}^{-1}$ and the corresponding angular frequency is $\omega_0 = 9.90\ \mathrm{s}^{-1}$. In the first set of experiments the nonlinearity is changed by varying $a = \{0.01, 0.02, 0.03\}$ m such that the wave steepness is $\epsilon = \{0.1, 0.2, 0.3\}$. Forcing and constant damping are set as $\Gamma = D(\omega_0) = 7.6 \times 10^{-3}\ \mathrm{m}^{-1}$, achieved by setting $\alpha_3 = 7.6 \times 10^{-6}\ \mathrm{s}^3\mathrm{m}^{-1}$. Note that for heterogeneous damping, this choice results in an overall weak damping. In the second set of experiments the forcing and damping strengths are 0.1, 0.3 and 0.7 times the original Γ and $D(\omega_0)$ but we only focus on the largest level of nonlinearity $a = 0.03$ m ($\epsilon = 0.3$).

The boundary condition at $x = 0$ (we recall that Eq. (1) is an evolution equation in x) is:

$$a_0(t) = \frac{\epsilon}{k_0}\mathrm{sech}\Big(-\frac{\sqrt{2}}{2}\epsilon\frac{k_0}{\omega_0}t\Big). \tag{4}$$

This solitonic solution generates a deterministic realisation of a broad banded spectrum, therefore allowing to track the dynamics of multiple interacting frequency modes. Moreover, this particular solution is known to be stable in the conservative NLS system [42], i.e. its shape does not change in space when no damping/forcing is applied, and evolves in space according to:

$$a(x,t) = \exp(ik_0x)a_0(t), \tag{5}$$

which provides a benchmark for our simulations.

We consider a spatial evolution over a domain of 62.9 m (equivalent to 100 wavelengths) and a periodic temporal domain of 63.3 s (equivalent to 100 wave periods). The periodic temporal domain enables us to efficiently compute the time derivative in frequency space. Consequently, the initial solution is evolved in space with a Runge–Kutta fourth order scheme (RK4). The time domain is discretised with $2^8+1 = 257$ points and the spatial domain with $2^{12}+1 = 4097$ points. All temporal derivatives are computed over the periodic domain using the fast Fourier transform algorithm which improves computational speed and reduces the necessary number of grid points when compared to finite element approaches. The spatial and temporal resolution were informed by numerical tests, it was found that the chosen spatial and temporal resolution preserve the balance between accuracy and computational speed.

3. Results

3.1. The effect of nonlinearity

The normalised intensity profile of waves generated for a fixed strength of damping are shown in Fig. 1. Time and space coordinates are made dimensionless, i.e. $T = \omega_0 t$ and $X = k_0 x$, as well as the amplitude, i.e. $A_0 = a_0(t = 0)$. The first and third rows show a single wave contour for the NLS and HONLS, respectively, and the line denotes the centre of the wave profile throughout the spatial evolution. The second and fourth rows show the centrelines for all values of the wave steepness. We note that the derivative of the drift denotes the speed of the envelope, e.g. no translation is equivalent to an envelope moving at the group speed, and a tilt to the left/right denotes an increase/decrease.

For the conservative case (Fig. 1a), the NLS wave envelope remains unchanged during the evolution, and for all values of the steepness (Fig. 1d), as expected. The same behaviour is observed for the HONLS but only when the steepness is low (see Fig. 1j). When the steepness increases the envelope first drifts to the left (Fig. 1j), therefore indicating acceleration compared to the group velocity, before decelerating.

For constant dissipation (Fig. 1b, e, h, k), the amplitude of the envelope decreases during propagation without any drift in the NLS (Fig. 1b; in analogy with the conservative case) but when HO terms are included it drifts to the left (a speed-up compared to the group velocity). For a given level of nonlinearity, the drift pattern in the HONLS with constant damping is similar but less intense to the HONLS without dissipation.

When heterogeneous dissipation is introduced, the NLS solution drifts rightward (Fig. 1c) therefore indicating a slow-down compared to the group velocity. The rate of slow-down depends on the wave steepness but not in a linear manner. The slow-down for the heterogeneous dissipation is counter-intuitive however, for the weak dissipation assumed in this study, the carrier wave component remains the same even after attenuation. Moreover, the slow-down of the envelope is in qualitative agreement with results of Alberello and Părău [36] for random sea state. Nevertheless, the expectation is that the envelope will speed-up when lower frequency are dissipated at higher rate. We could speculate that the observed slow-down is driven by the complex dynamical behaviour when left/right symmetry is broken [see 37] and/or a narrowing of the spectrum which do not occur for homogeneous damping, but a firmer theoretical explanation should be sought. The picture is more complicated when HO terms are included (Fig. 1g–i). In this case the envelope initially accelerates and then slows-down for the highest steepness (Fig. 1i). The change in drifting speed is less accentuated for lower levels of nonlinearity (Fig. 1l).

Intensity profiles when forcing is introduced are shown in Fig. 2. When only forcing is present there is an overall increase of energy and the amplitude of the envelope increases (Fig. 2a, d, g, j). However, when forcing is balanced by dissipation the energy of the system is approximately conserved (at least for constant damping; Fig. 2b, e, h, k) and, as a result the profiles do not undergo significant reduction during propagation (also seen in Fig. 2c, f, i, l).

In the NLS the drift is absent when only forcing is present (Fig. 2a), similar to the case of no forcing and no dissipation. However, in the HONLS, forcing induces an acceleration (leftward shift) which is stronger for increasing steepness (Fig. 2j) but less intense than in the absence of forcing (cf. Fig. 1j). When forcing and damping are balanced (Fig. 2b, e, h, k) no drift is observed in the NLS system but a leftward shift (acceleration) is shown in the HONLS. Compared to the case without wind forcing, the drift is accentuated (cf. Fig. 2k). When frequency-dependent attenuation is used in combination with wind forcing (Fig. 2c, f, i, l) the drifting patterns are varied, i.e. it alternates faster and the envelope has a slower velocity, in both the NLS and HONLS system but it appears that an

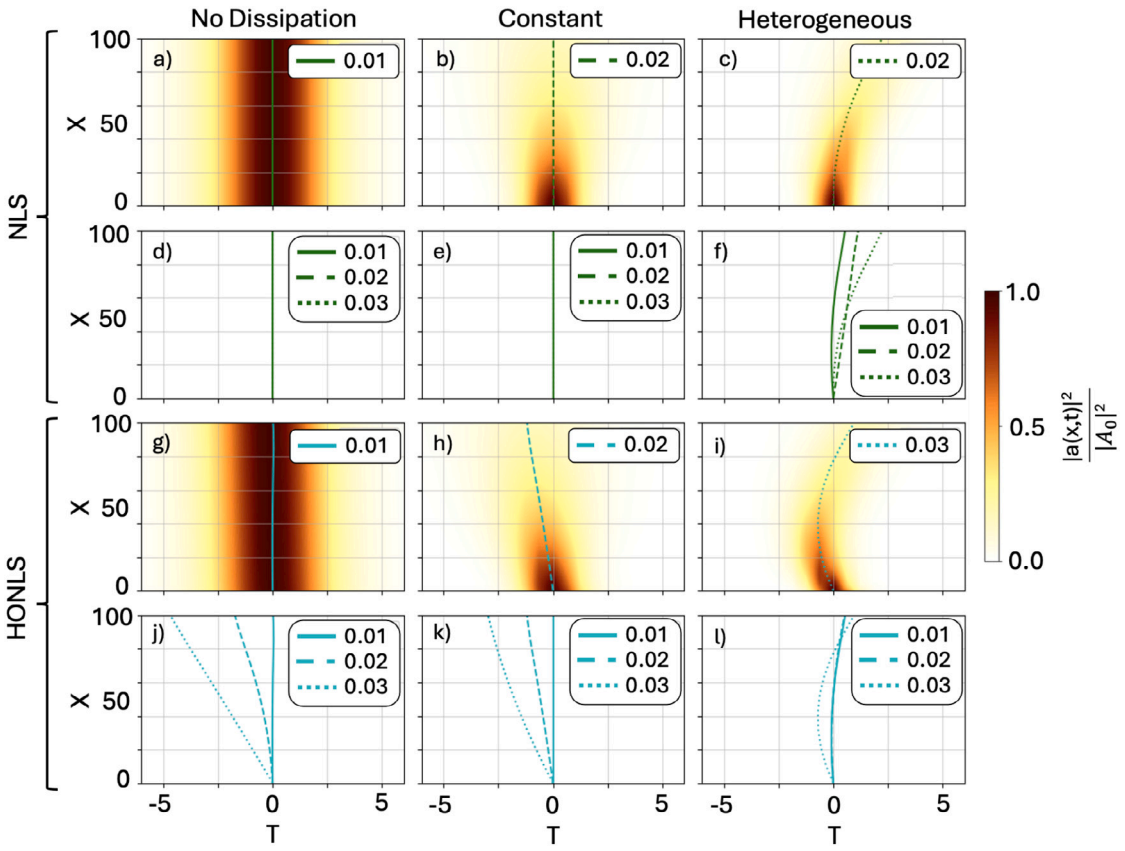

Fig. 1. Wave envelopes in the NLS and HONLS with a fixed value of damping and no forcing. Each column displays results for a different type of damping: none, constant, and heterogeneous. Lines show the maximum amplitude for a given position (X). Amplitudes $\{0.01, 0.02, 0.03\}$ m are denoted by solid, dashed, and dotted linestyles respectively and model by colour (NLS in green, HONLS in cyan). (For interpretation of the references to colour in this figure legend, the reader is referred to the web version of this article.)

overall slight rightward drift occurs by the end of the spatial domain. However, a clear pattern with initial wave steepness is hard to discern.

In the cases in which the forcing is present it is interesting to look at the width of the envelope. When no dissipation is present (Fig. 2a, d, g, j) the envelope widens and shrinks in agreement with the NLS and HONLS dynamics and the only difference appears to be the overall drift; which is in contrast to the case without forcing in which it remains constant (see also Fig. A.2 in the Supplementary Information). Periodic shrinking and widening is also observed in the HONLS when forcing and heterogeneous dissipation are present (Fig. 2l). The analysis of the asymmetry reveals how profiles remain symmetric when homogeneous dissipation is applied (also in case of forcing) however the frequency dependent dissipation promotes the development of a skewed profile. This is more intense for high nonlinearity (see also SI Fig. A.3).

For a few representative cases in which attenuation is balanced by the forcing we showcase the spatial evolution of the wave spectrum (see Fig. 3). In all cases, the carrier wave does not shift (we recall that for all cases the dissipation is weak), but an oscillating pattern emerges in the HONLS, highlighting a more complex behaviour.

The difference between left (low frequency components; $\Omega < 0$ where $\Omega = \omega/\omega_0$) and right (high frequency components; $\Omega < 0$) are showcased in Fig. 4, where the normalised energy is shown, i.e.:

$$E_{\text{left}}(X) = \frac{\int_{-\infty}^{0^-} |\tilde{a}(X;\Omega)|^2 \, \mathrm{d}\Omega}{\int_{-\infty}^{0^-} |\tilde{a}(0;\Omega)|^2 \, \mathrm{d}\Omega}; \quad E_{\text{right}}(X) = \frac{\int_{0^+}^{\infty} |\tilde{a}(X;\Omega)|^2 \, \mathrm{d}\Omega}{\int_{0^+}^{\infty} |\tilde{a}(0;\Omega)|^2 \, \mathrm{d}\Omega}, \tag{6}$$

where $\{\tilde{\cdot}\}$ and $\mathcal{F}[\{\cdot\}]$ are used interchangeably. In the NLS with constant dissipation both right and left energy overlap, and both grow with slight oscillations reminiscent of recurrence observed in Alberello et al. [37]. When heterogeneous dissipation is introduced symmetry between the low and high frequency side of the spectrum is broken. At early stages of the evolution the low frequency components grow while the high frequency components decrease, and a complex interplay of energy exchanges occur at later stages. The difference between right and left components are enhanced in the HONLS simulations, and also for constant dissipation the two sides of the spectrum behave differently, i.e. low frequencies grow while high frequencies decrease. This behaviour, for constant dissipation, is due to the energy cascade towards low frequencies which occurs by including HO terms. The presence

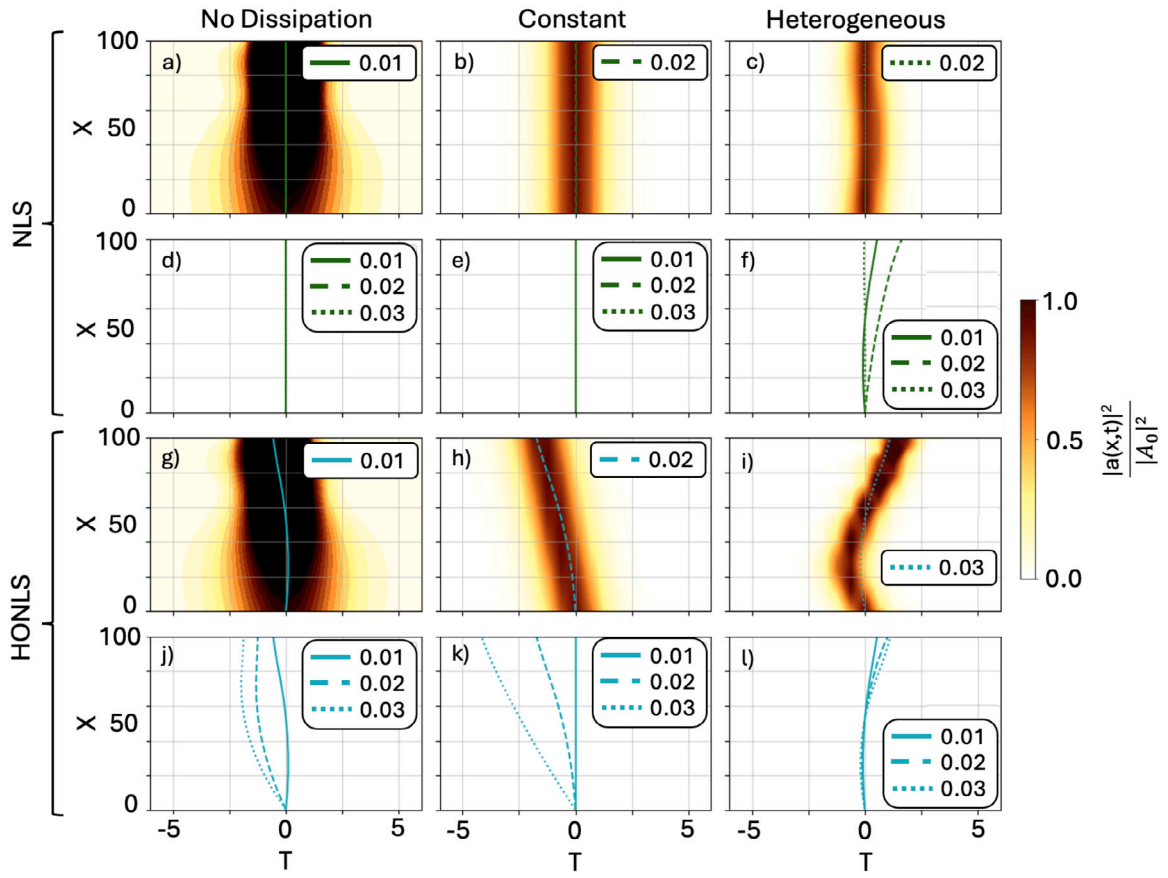

Fig. 2. Same as in Fig. 1 but for wave profiles with damping and forcing.

of heterogeneous damping in the HONLS enhances differences and the complex interplay between energy components as already displayed in Fig. 3.

The energy exchanges, dI, for a few representative cases are shown in Fig. 5 for the NLS and Fig. 6 for the HONLS. As in the previous case, only cases in which damping and forcing are balanced are displayed to showcase the system close to energetic equilibrium (other cases would be dominated by dissipation). These are quantified from the difference in frequency spectra:

$$I(\Omega) = |\tilde{a}(0;\Omega)|^2 - |\tilde{a}(X;\Omega)|^2 \equiv \left|\mathcal{F}\left[a(0)\right]\right|^2 - \left|\mathcal{F}\left[a(X)\right]\right|^2. \tag{7}$$

In particular, the line plots depict $dI(\Omega) = \sum_X I(\Omega)$. Positive values are associated to damping (loss) and negative values to gain. The line plot shows the exchange rate over the entire spatial domain.

In the NLS, the asymmetry in gain/losses clearly highlights the frequency dependent dissipation (Fig. 5a and c) which contrast the case of homogeneous damping. In the HONLS, asymmetry in gain/losses between left and right modes is already present for constant damping due to the presence of the HO terms which promote energy exchanges to the left. The presence of heterogeneous dissipation enhances the asymmetry between left and right modes. This is particularly evident in the profiles in which the right modes are subjected to gain and left sideband to loss (Fig. 6d).

3.2. The effect of damping/forcing strength

In the next section we address the change in wave dynamics for a fixed value of the wave steepness. Figs. 7 and 8 presents the wave profiles of the NLS and HONLS without and with wind forcing, respectively, for reduced level of damping (70%, 30%, and 10% of the original damping strength).

For the conservative case, Fig. 7a, the wave profile remains constant throughout the course of the evolution, in agreement with Fig. 1a. For all values of the damping there is a strong, constant, acceleration resulting in a leftward drift of the envelope (Fig. 7g-j), i.e. drift only depends on steepness. For the constant dissipation (Fig. 7b, e, h, k) the NLS dissipates energy, resulting in a decreased peak amplitude, with an increased width, but the envelope travels at group velocity. However, in the HONLS drift depends on the strength of the damping (Fig. 7k). For greater damping the loss of energy is more substantial, and as a consequence nonlinearity

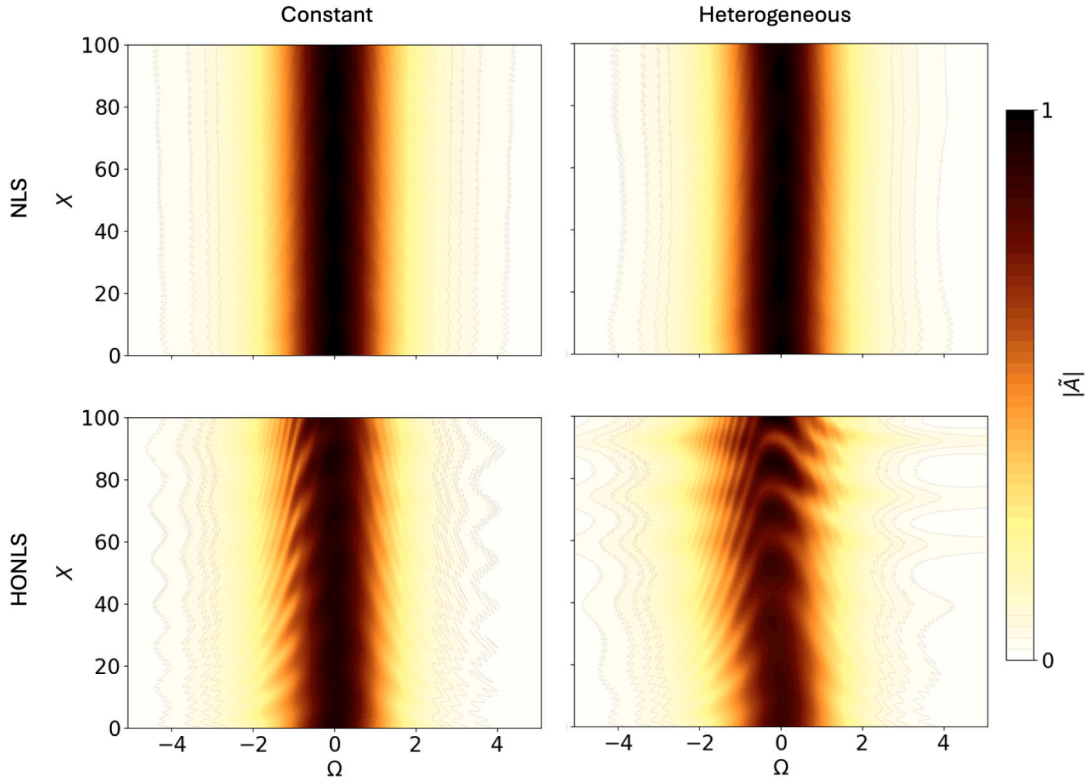

Fig. 3. Energy spectrum for waves with dissipation and with wind forcing as a function of propagation distance. First row for the NLS, second row the HONLS. Left column for constant, right for heterogeneous dissipation.

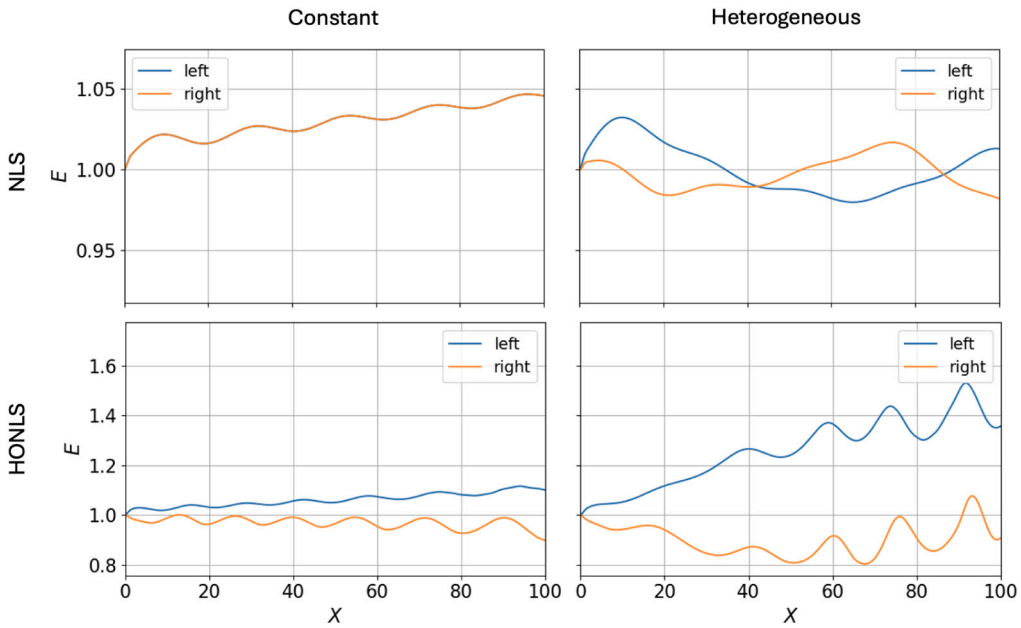

Fig. 4. Spatial evolution of left and right ($\Omega > 0$) integrated energy with dissipation and with wind forcing. First row for the NLS, second row the HONLS. Left column for constant, right for heterogeneous dissipation.

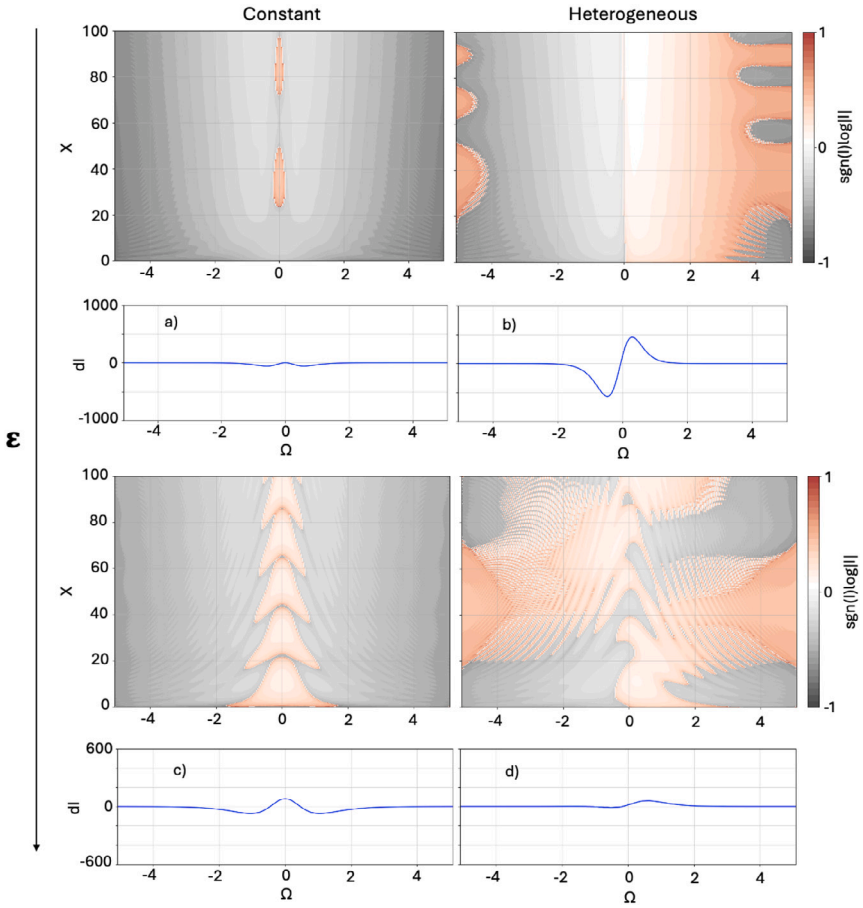

Fig. 5. Energy exchange rate for NLS with forcing. The first column presents results with a constant damping rate, and the second column those with a heterogeneous damping rate. Moving down the column denotes an increase in the steepness from 0.2 to 0.3. Each contour has an associated line plot, showing the change in I over the spatial domain, denoted dI.

decreases faster therefore reducing the difference with the NLS model.

When the heterogeneous dissipation is introduced there is a change in the drift of both the NLS and HONLS models. In agreement with Fig. 1, the NLS model decelerates, with the largest deceleration occurring for the largest value of damping (Fig. 7f). However, for the smallest dissipation the wave envelope remains at the group velocity for the entire propagation. Importantly, the NLS model never exhibits any leftward drift for the chosen boundary condition. In contrast, the HO terms in the HONLS allow the profiles to initially accelerate (Fig. 7l) and then decelerate (this is linked to the presence of the explicit dependency on amplitude in the HO terms which breaks the left/right symmetry), but only when damping is more substantial.

Fig. 8 shows the effect of wind forcing. In analogy with Fig. 2, the presence of the balancing term induces an acceleration of the profile but the width and asymmetry are less impacted. In the HONLS model the drift speed depends on wind forcing (Fig. 8j), this is because the absence of the damping term allows for an overall growth of the energy and consequently an increase in the nonlinearity. On the other hand, with constant damping the spread in drift is reduced. For an heterogeneous damping rate with wind forcing the NLS solution does not undergo any drift in contrast to the case without wind (Fig. 7) but the results are qualitatively similar in the HONLS case. The width of the envelope with and without wind forcing (Figs. 7 and 8) for varying levels of the damping/forcing strength are in qualitative agreement with the results for varying wave steepness (Figs. 1 and 2).

A comparison between the energy exchange rates for the constant and heterogeneous damping rates is shown in Figs. 9 and 10. When only damping is applied, a net loss is obtained. The NLS energy exchange profiles for constant damping, Fig. 9a, is symmetric. Both NLS panels show that the model is dominated by the leading energetic dissipation. In contrast, Fig. 9c and d for the HONLS, presents strongly asymmetric energy exchange contours due to the HO terms. As a results the right modes are less dissipative than the left modes when constant damping is applied. The presence of heterogeneous damping, higher for the right modes, flips the situation. When wind is introduced to restore the balance (Fig. 10) the effect of the HO terms have a magnified impact on the dynamics in the case of constant damping as highlighted by the differences between top and bottom panels (Fig. 10a–b vs Fig. 10c–d). For heterogeneous damping, asymmetry also emerges in the NLS but the overall effect is neutral over the entire domain, i.e. dI is close to 0 for all frequencies. This is in stark contrast to the HONLS with heterogeneous damping in which right modes show a

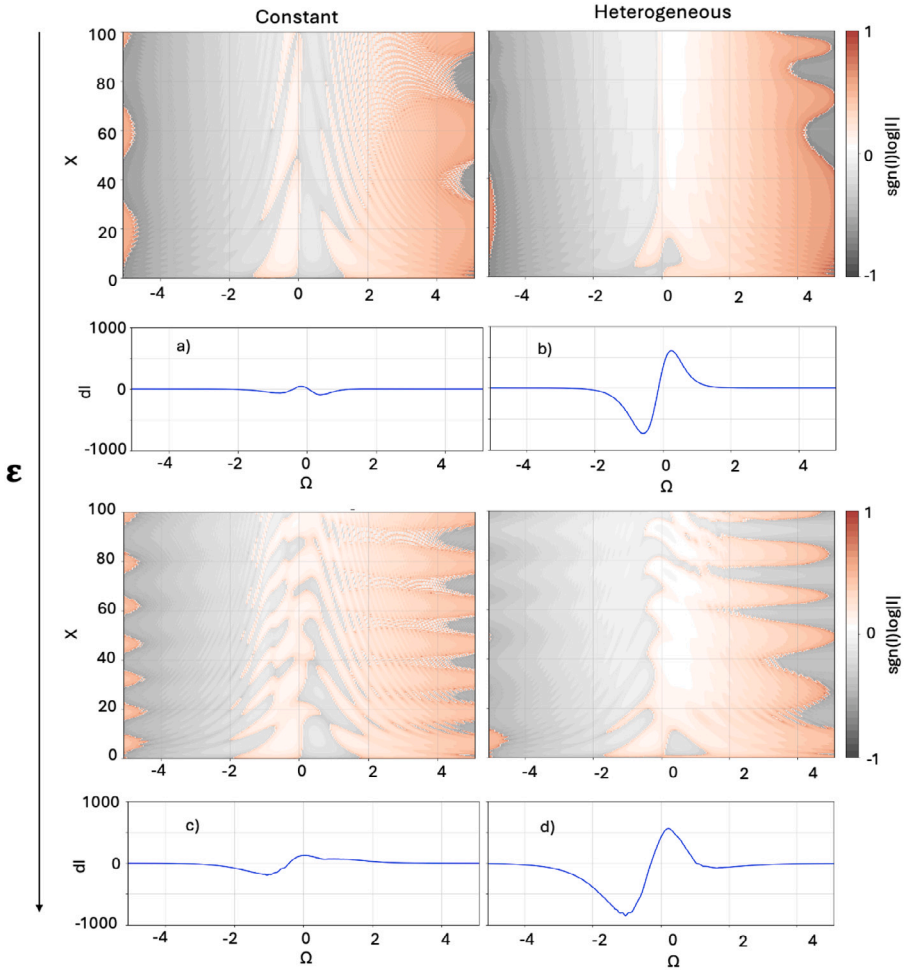

Fig. 6. Same as in Fig. 5 but for the HONLS.

net loss, and left modes a net gain.

4. Conclusions

The dynamics of nonlinear waves have been modelled with the NLS and HONLS under the effect of forcing and heterogeneous damping has been assessed. This constitutes an advancement of previous studies in which either lower order models (NLS) and frequency dependent damping [37] or HONLS and constant damping have been considered [18,28,29]. In agreement with previous studies of heterogeneous damping [31,37] it has been shown that a cubic frequency dependence induces a spectral asymmetry. However, here we highlight that, when forcing is present to generate an energetic equilibrium, the impact of HO terms is magnified and the wave dynamics are profoundly impacted — the effect of HO terms is less obvious when only dissipation is present as the dynamics are dominated by the loss of energy. One of the features is that for the NLS model only deceleration of the envelope can be achieved for the chosen solitonic boundary condition. While we could speculate on the reasons of the slow-down of the envelope in the NLS when only dissipation is present, a firmer theoretical explanation should be sought. In the HONLS the dynamics are more varied and acceleration is possible under certain combinations of wave steepness and strength of the forcing/dissipation due to the presence of HO terms that enhance energy exchanges between wave components and promote a richer dynamical behaviour. In particular, as the wave steepness increases, so does the degree of nonlinearity, but only the presence of HO terms allows the wave envelope to speed-up. In summary, inclusion of heterogeneous damping and HO is imperative when the system is close to a net energetic equilibrium to accurately capture the complex dynamics.

While the paper focused on ocean waves under the action of wind forcing and dissipation as the one found in sea ice (ω^n), we expect the results to have broader applicability. We believe that heterogeneous dissipation might be a better representation of physical systems such as ocean wave dynamics [31], physical optics [3,4], and metamaterials [9].

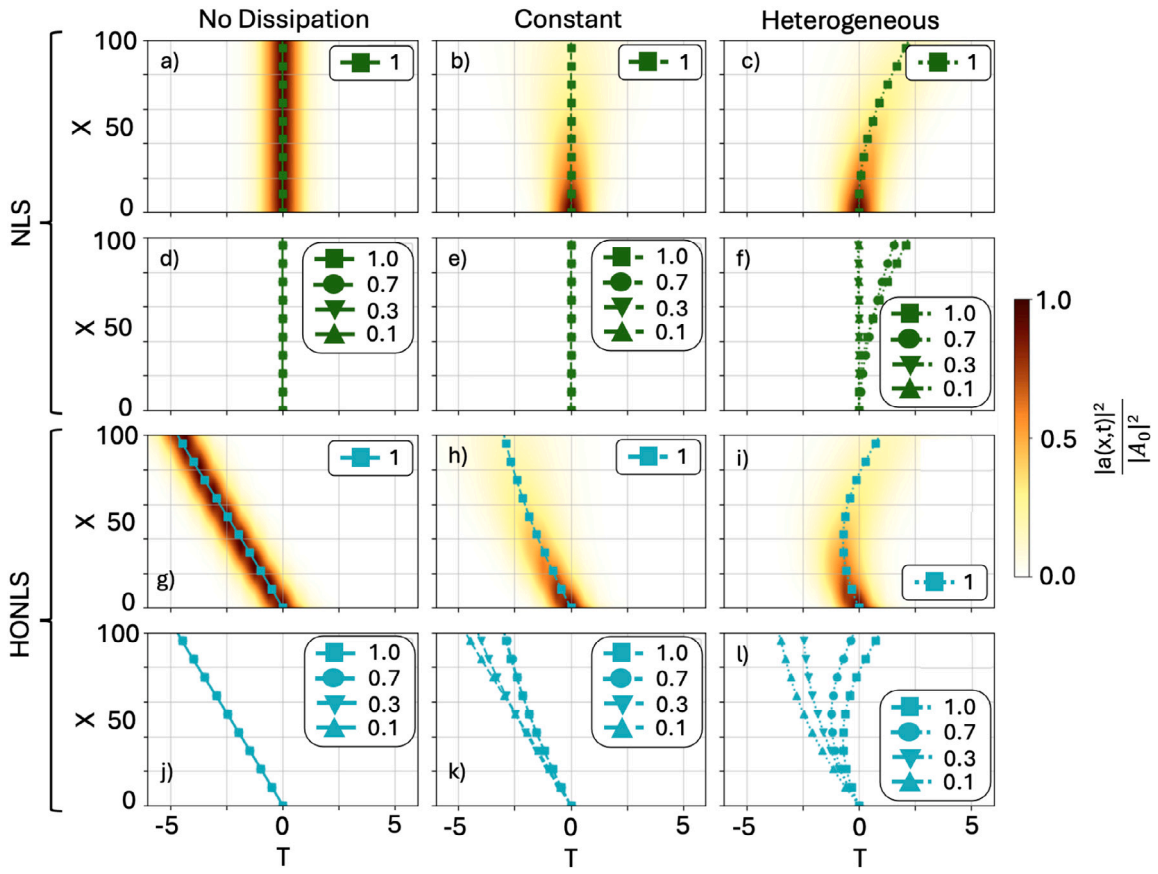

Fig. 7. Wave envelopes for $\epsilon = 0.3$ without forcing in the NLS and HONLS. Each column displays results for a different type of damping: none, constant, and heterogeneous. Lines show the maximum amplitude for a given position (X). The four markerstyles: {square, circle, triangle down, triangle up} denote $\{100, 70, 30, 10\}$% damping rates. Model is denoted by colour (NLS in green, HONLS in cyan). (For interpretation of the references to colour in this figure legend, the reader is referred to the web version of this article.)

In future works it would be interesting to explore the effect of even values of n, that will result in dissipation with only real part and might generate a different dynamics, and non-integer n (within Eq. (3)) leading to non-local damping. It would also be interesting to extend the analysis of Eeltink et al. [30] and Stuhlmeier et al. [40] of a three mode system by adding asymmetric damping and forcing. In the context of waves in ice, the inclusion of inertial effects, as done by Slunyaev and Stepanyants [39], would enable to analysis of waves transitioning from the exterior of the marginal ice zone to the interior zone.

CRediT authorship contribution statement

Ben S. Humphries: Writing – review & editing, Writing – original draft, Visualization, Software, Methodology, Investigation, Formal analysis, Data curation. **Jack S. Keeler:** Writing – review & editing, Writing – original draft, Investigation, Formal analysis. **Alberto Alberello:** Writing – review & editing, Writing – original draft, Supervision, Project administration, Methodology, Investigation, Funding acquisition, Formal analysis, Data curation, Conceptualization. **Emilian I. Părău:** Writing – review & editing, Writing – original draft, Supervision, Project administration, Investigation, Funding acquisition, Formal analysis, Conceptualization.

Declaration of competing interest

The authors declare that they have no known competing financial interests or personal relationships that could have appeared to influence the work reported in this paper.

Acknowledgements

We acknowledge funding from EPSRC, United Kingdom (EP/Y02012X/1). JSK acknowledges funding from the Leverhulme Trust, United Kingdom (ECF-2021-017). BSH acknowledges support from the Institute of Mathematics and Applications through the

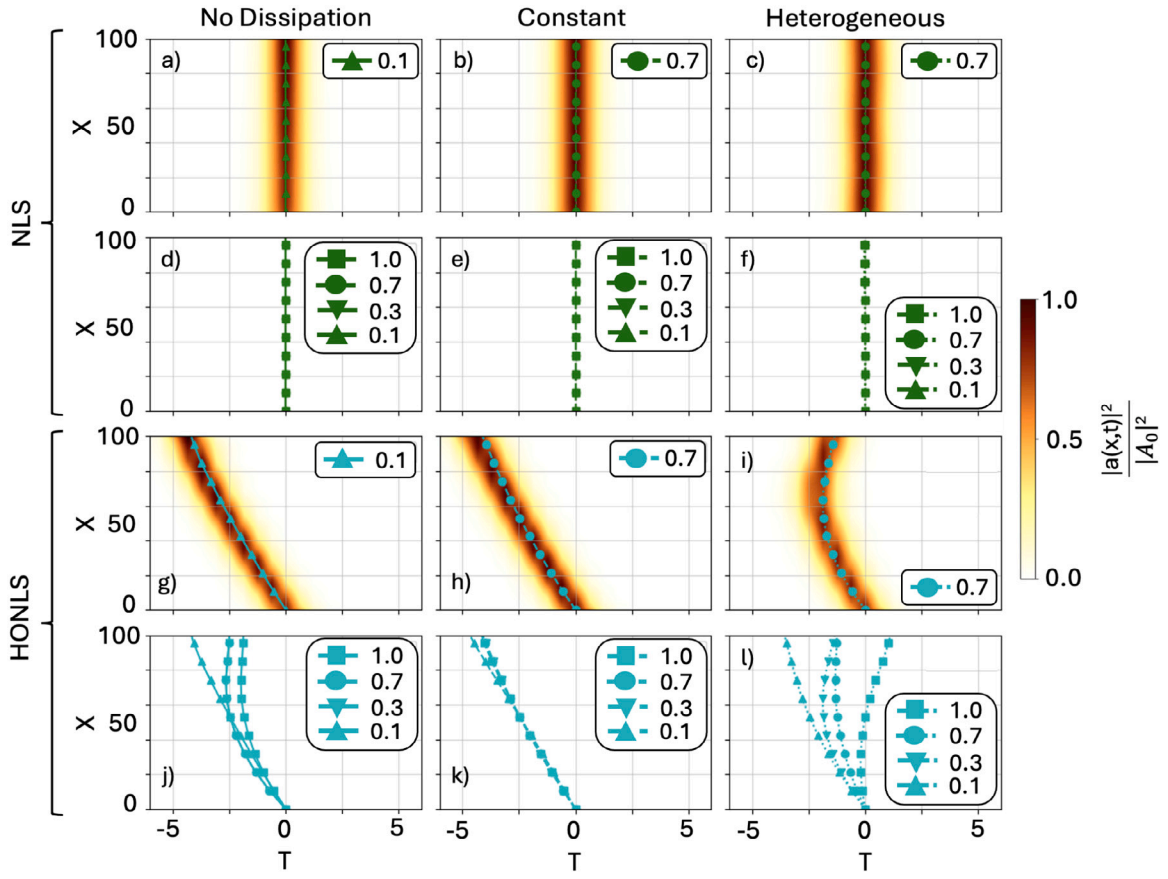

Fig. 8. Same as in Fig. 7 but with forcing.

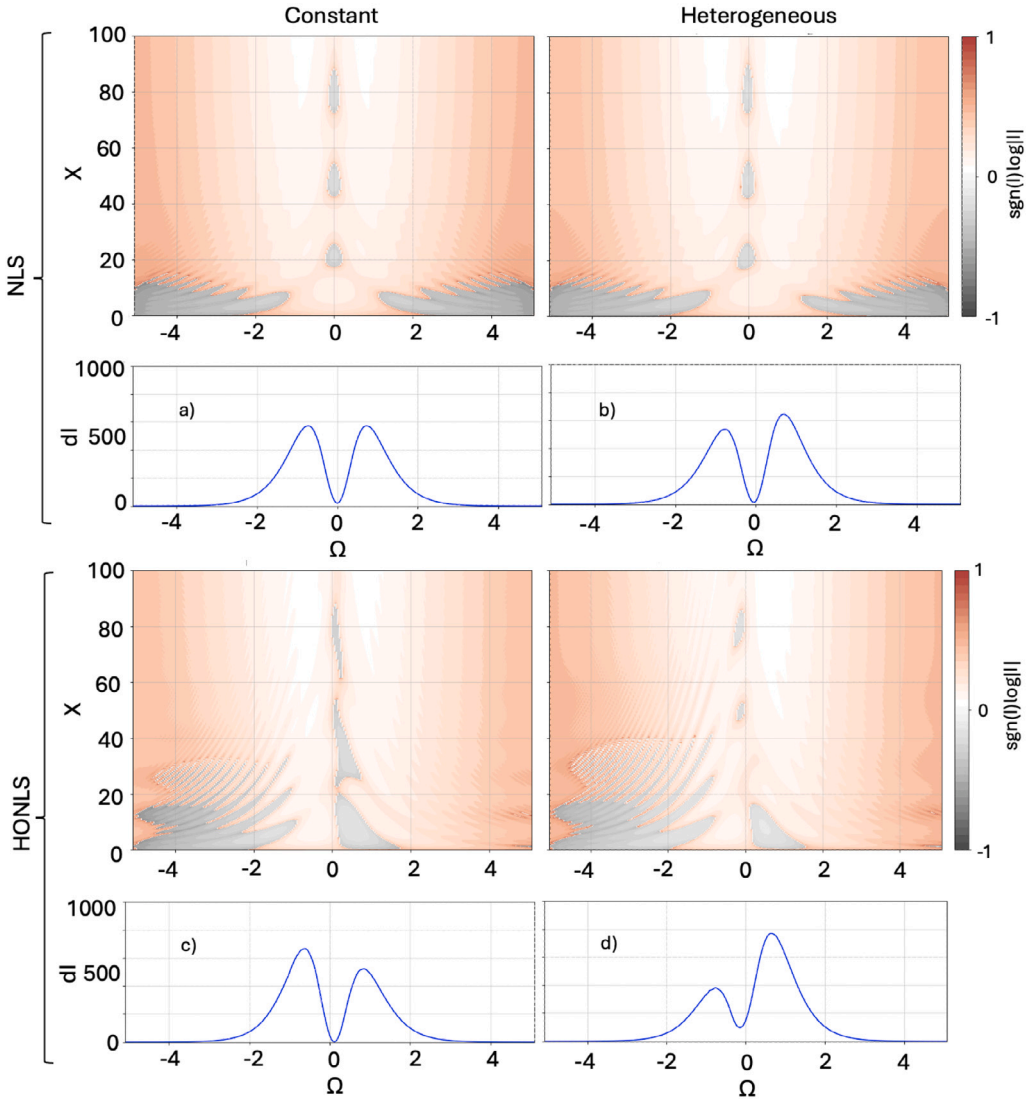

Fig. 9. Energy exchange for the NLS (a) and (b), and HONLS (c) and (d) with dissipation set to 30% and no forcing. Left column for constant, right for heterogeneous dissipation.

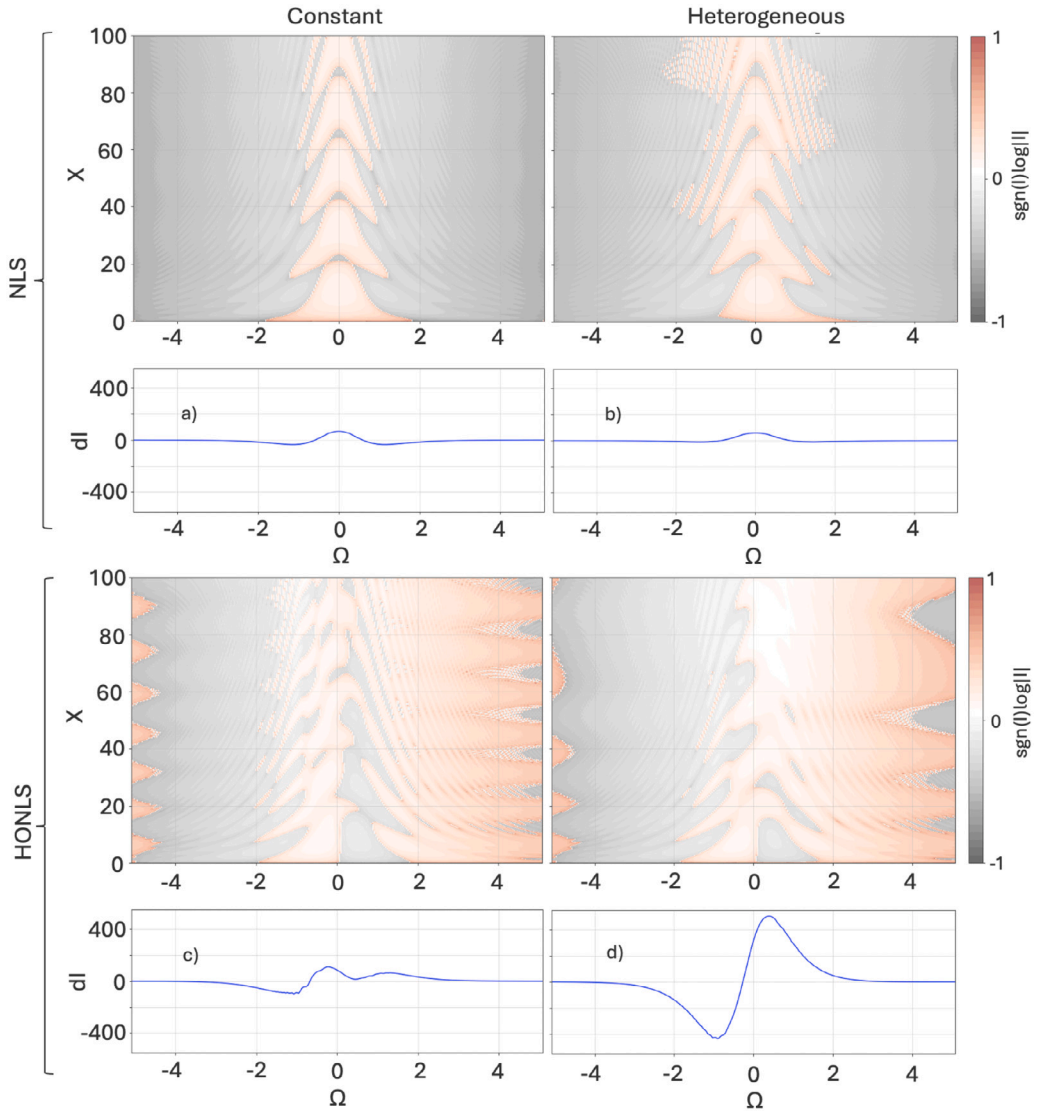

Fig. 10. Same as Fig. 9 but for dissipation and wind forcing set to 30%.

QJMAM Fund for Applied Mathematics. The authors thank Prof M. Onorato and Dr D. Maestrini for fruitful discussions. The research presented in this paper was carried out on the High Performance Computing Cluster supported by the Research and Specialist Computing Support service at the University of East Anglia.

Appendix A. Supplementary data

Supplementary material related to this article can be found online at https://doi.org/10.1016/j.wavemoti.2024.103482.

Data availability

Data will be made available on request.

References

[1] Usman Younas, T.A. Sulaiman, Jingli Ren, On the study of optical soliton solutions to the three-component coupled nonlinear Schrödinger equation: applications in fiber optics, Opt. Quantum Electron. (ISSN: 1572817X) 55 (1) (2023) 1–11, http://dx.doi.org/10.1007/s11082-022-04254-x,

[2] Masao Nagasawa, Schrödinger Equations and Diffusion Theory, Springer Basel, Basel, ISBN: 978-3-0348-0559-9, 1993, http://dx.doi.org/10.1007/978-3-0348-0560-5, URL https://link.springer.com/10.1007/978-3-0348-0560-5.

[3] T. Herr, V. Brasch, J.D. Jost, C.Y. Wang, N.M. Kondratiev, M.L. Gorodetsky, T.J. Kippenberg, Temporal solitons in optical microresonators, Nat. Photonics (ISSN: 1749-4885) 8 (2) (2014) 145–152, http://dx.doi.org/10.1038/nphoton.2013.343, URL https://www.nature.com/articles/nphoton.2013.343.

[4] Hui Deng, Hartmut Haug, Yoshihisa Yamamoto, Exciton-polariton Bose-Einstein condensation, Rev. Modern Phys. (ISSN: 00346861) 82 (2) (2010) 1489–1537, http://dx.doi.org/10.1103/RevModPhys.82.1489.

[5] Harold Conroy, Molecular Schrödinger equation. VIII. A new method for the evaluation of multidimensional integrals, J. Chem. Phys. (ISSN: 00219606) 47 (12) (1967) 5307–5318, http://dx.doi.org/10.1063/1.1701795.

[6] Gennady El, Alexander Tovbis, Spectral theory of soliton and breather gases for the focusing nonlinear Schrödinger equation, Phys. Rev. E (ISSN: 2470-0045) 101 (5) (2020) 052207, http://dx.doi.org/10.1103/PhysRevE.101.052207, URL https://link.aps.org/doi/10.1103/PhysRevE.101.052207.

[7] Padma K. Shukla, B. Eliasson, Nonlinear aspects of quantum plasma physics, Phys.-Usp. (ISSN: 1063-7869) 53 (1) (2010) 51–76, http://dx.doi.org/10.3367/ufne.0180.201001b.0055, arXiv:0906.4051.

[8] Catherine Sulem, Pirre-Louis Sulem, The Nonlinear Schrödinger Equation: Self-Focusing and Wave Collapse, in: Applied Mathematical Sciences, vol. 139, Springer New York, New York, NY, ISBN: 978-0-387-98611-1, 1999, http://dx.doi.org/10.1007/b98958, URL http://link.springer.com/10.1007/b98958.

[9] A. Demiquel, V. Achilleos, G. Theocharis, V. Tournat, Modulation instability in nonlinear flexible mechanical metamaterials, Phys. Rev. E (ISSN: 24700053) 107 (5) (2023) 38–44, http://dx.doi.org/10.1103/PhysRevE.107.054212.

[10] François Copie, Stéphane Randoux, Pierre Suret, The Physics of the one-dimensional nonlinear Schrödinger equation in fiber optics: Rogue waves, modulation instability and self-focusing phenomena, Rev. Phys. (ISSN: 24054283) 5 (July 2019) (2020) 100037, http://dx.doi.org/10.1016/j.revip.2019.100037.

[11] Miguel Onorato, Stefania Resitori, Fabio Baronio (Eds.), Rogue and Shock Waves in Nonlinear Dispersive Media, in: Lecture Notes in Physics, vol. 926, Springer International Publishing, Cham, ISBN: 978-3-319-39212-7, 2016, http://dx.doi.org/10.1007/978-3-319-39214-1, URL http://link.springer.com/10.1007/978-3-319-39214-1.

[12] Ricardo Grande, Space-time fractional nonlinear Schrödinger equation, SIAM J. Math. Anal. (ISSN: 0036-1410) 51 (5) (2019) 4172–4212, http://dx.doi.org/10.1137/19M1247140, URL https://epubs.siam.org/doi/10.1137/19M1247140.

[13] A. Barchielli, C. Pellegrini, F. Petruccione, Stochastic Schrödinger equations with coloured noise, EPL (Europhys. Lett. (ISSN: 0295-5075) 91 (2) (2010) 24001, http://dx.doi.org/10.1209/0295-5075/91/24001, URL https://iopscience.iop.org/article/10.1209/0295-5075/91/24001.

[14] Abner Shimony, Proposed neutron interferometer test of some nonlinear variants of wave mechanics, Phys. Rev. A (ISSN: 0556-2791) 20 (2) (1979) 394–396, http://dx.doi.org/10.1103/PhysRevA.20.394, URL https://link.aps.org/doi/10.1103/PhysRevA.20.394.

[15] Garth A. Jones, David S. Bradshaw, Resonance energy transfer: From fundamental theory to recent applications, Front. Phys. (ISSN: 2296-424X) 7 (JULY) (2019) 1–19, http://dx.doi.org/10.3389/fphy.2019.00100, URL https://www.frontiersin.org/article/10.3389/fphy.2019.00100/full.

[16] Jinbing Chen, Dmitry E. Pelinovsky, Rogue waves on the background of periodic standing waves in the derivative nonlinear Schrödinger equation, Phys. Rev. E (ISSN: 2470-0045) 103 (6) (2021) 062206, http://dx.doi.org/10.1103/PhysRevE.103.062206, URL https://link.aps.org/doi/10.1103/PhysRevE.103.062206.

[17] Aly R. Seadawy, Muhammad Arshad, Dianchen Lu, The weakly nonlinear wave propagation of the generalized third-order nonlinear Schrödinger equation and its applications, Waves Random Complex Media (ISSN: 1745-5030) 32 (2) (2022) 819–831, http://dx.doi.org/10.1080/17455030.2020.1802085, URL https://www.tandfonline.com/doi/full/10.1080/17455030.2020.1802085.

[18] Andrea Armaroli, Debbie Eeltink, Maura Brunetti, Jérôme Kasparian, Viscous damping of gravity-capillary waves: Dispersion relations and nonlinear corrections, Phys. Rev. Fluids (ISSN: 2469-990X) 3 (12) (2018) 124803, http://dx.doi.org/10.1103/PhysRevFluids.3.124803, URL https://link.aps.org/doi/10.1103/PhysRevFluids.3.124803.

[19] M. Onorato, S. Residori, U. Bortolozzo, A. Montina, F.T. Arecchi, Rogue waves and their generating mechanisms in different physical contexts, Phys. Rep. (ISSN: 03701573) 528 (2) (2013) 47–89, http://dx.doi.org/10.1016/j.physrep.2013.03.001.

[20] V.E. Zakharov, L.A. Ostrovsky, Modulation instability: The beginning, Phys. D Nonlinear Phenom. (ISSN: 01672789) 238 (5) (2009) 540–548, http://dx.doi.org/10.1016/j.physd.2008.12.002, URL https://linkinghub.elsevier.com/retrieve/pii/S0167278908004223.

[21] K.B. Dysthe, Note on a modification to the nonlinear Schrödinger equation for application to deep water waves, Proc. R. Soc. Lond. A Math. Phys. Sci. (ISSN: 0080-4630) 369 (1736) (1979) 105–114, http://dx.doi.org/10.1098/rspa.1979.0154, URL https://royalsocietypublishing.org/doi/10.1098/rspa.1979.0154.

[22] F. Dias, A.I. Dyachenko, V.E. Zakharov, Theory of weakly damped free-surface flows: A new formulation based on potential flow solutions, Phys. Lett. Sect. A Gen. At. Solid State Phys. (ISSN: 03759601) 372 (8) (2008) 1297–1302, http://dx.doi.org/10.1016/j.physleta.2007.09.027, arXiv:0704.3352.

[23] Harvey Segur, Diane Henderson, John Carter, Joe Hammack, Cong-Ming Li, Dana Pheiff, Katherine Socha, Stabilizing the Benjamin–Feir instability, J. Fluid Mech. (ISSN: 0022-1120) 539 (2005) 229, http://dx.doi.org/10.1017/S002211200500563X, URL http://www.journals.cambridge.org/abstract_S002211200500563X.

[24] Guangyu Wu, Yuming Liu, Dick K.P. Yue, A note on stabilizing the Benjamin–Feir instability, J. Fluid Mech. (ISSN: 0022-1120) 556 (2006) 45, http://dx.doi.org/10.1017/S0022112005008293, URL http://www.journals.cambridge.org/abstract_S0022112005008293.

[25] Miguel Onorato, Davide Proment, Approximate rogue wave solutions of the forced and damped nonlinear Schrödinger equation for water waves, Phys. Lett. A (ISSN: 03759601) 376 (45) (2012) 3057–3059, http://dx.doi.org/10.1016/j.physleta.2012.05.063, URL https://linkinghub.elsevier.com/retrieve/pii/S0375960112008377.

[26] Leo Dostal, The Effect of Random Wind Forcing in the Nonlinear Schrödinger Equation, Fluids (ISSN: 2311-5521) 4 (3) (2019) 121, http://dx.doi.org/10.3390/fluids4030121, URL https://www.mdpi.com/2311-5521/4/3/121.

[27] Bo Liao, Guohai Dong, Yuxiang Ma, Xiaozhou Ma, Marc Perlin, Modified nonlinear Schrödinger equation for gravity waves with the influence of wind, currents, and dissipation, Phys. Fluids (ISSN: 10897666) 35 (3) (2023) http://dx.doi.org/10.1063/5.0137966.

[28] D. Eeltink, A. Lemoine, H. Branger, O. Kimmoun, C. Kharif, J.D. Carter, A. Chabchoub, M. Brunetti, J. Kasparian, Spectral up- and downshifting of Akhmediev breathers under wind forcing, Phys. Fluids (ISSN: 10897666) 29 (10) (2017) http://dx.doi.org/10.1063/1.4993972, arXiv:1709.09381.

[29] John D. Carter, Alex Govan, Frequency downshift in a viscous fluid, Eur. J. Mech. B Fluids (ISSN: 09977546) 59 (2016) 177–185, http://dx.doi.org/10.1016/j.euromechflu.2016.06.002, arXiv:1601.03932.

[30] D. Eeltink, A. Armaroli, C. Luneau, H. Branger, M. Brunetti, J. Kasparian, Separatrix crossing and symmetry breaking in NLSE-like systems due to forcing and damping, Nonlinear Dynam. (ISSN: 1573269X) 102 (4) (2020) 2385–2398, http://dx.doi.org/10.1007/s11071-020-06043-1, arXiv:2005.03931,

[31] M.H. Meylan, L.G. Bennetts, J.E.M. Mosig, W.E. Rogers, M.J. Doble, M.A. Peter, Dispersion relations, power laws, and energy loss for waves in the marginal ice zone, J. Geophys. Res. Ocean. (ISSN: 21699291) 123 (5) (2018) 3322–3335, http://dx.doi.org/10.1002/2018JC013776.

[32] Alison L. Kohout, Madison Smith, Lettie A. Roach, Guy Williams, Fabien Montiel, Michael J.M. Williams, Observations of exponential wave attenuation in Antarctic sea ice during the PIPERS campaign, Ann. Glaciol. (ISSN: 0260-3055) 61 (82) (2020) 196–209, http://dx.doi.org/10.1017/aog.2020.36, URL https://www.cambridge.org/core/product/identifier/S0260305520000361/type/journal_article.

[33] Takuji Waseda, A. Alberello, Takehiko Nose, Takenobu Toyota, Tsubasa Kodaira, Yasushi Fujiwara, Observation of anomalous spectral downshifting of waves in the Okhotsk Sea Marginal Ice Zone, Philos. Trans. R. Soc. A Math. Phys. Eng. Sci. (ISSN: 1364-503X) 380 (2235) (2022) http://dx.doi.org/10.1098/rsta.2021.0256, URL https://royalsocietypublishing.org/doi/10.1098/rsta.2021.0256.

[34] A. Toffoli, J.P.A. Pitt, A. Alberello, L.G. Bennetts, Modelling attenuation of irregular wave fields by artificial ice floes in the laboratory, Philos. Trans. R. Soc. A Math. Phys. Eng. Sci. (ISSN: 1364-503X) 380 (2235) (2022) http://dx.doi.org/10.1098/rsta.2021.0255, URL https://royalsocietypublishing.org/doi/10.1098/rsta.2021.0255.

[35] Francesca De Santi, Marcello Vichi, Alberto Alberello, Estimation of antarctic sea ice thickness through observation of wave attenuation, Ocean Model. (ISSN: 1463-5003) 191 (2024) 102421, http://dx.doi.org/10.1016/j.ocemod.2024.102421, URL https://www.sciencedirect.com/science/article/pii/S1463500324001082.

[36] A. Alberello, E.I. Părău, A dissipative nonlinear Schrödinger model for wave propagation in the marginal ice zone, Phys. Fluids (ISSN: 1070-6631) 34 (6) (2022) http://dx.doi.org/10.1063/5.0089866.

[37] A. Alberello, Emilian Părău, Amin Chabchoub, The dynamics of unstable waves in sea ice, Sci. Rep. (ISSN: 20452322) 13 (1) (2023) 1–11, http://dx.doi.org/10.1038/s41598-023-40696-3,

[38] A.V. Slunyaev, Y.A. Stepanyants, Frequency downshifting in decaying wavetrains on the ocean surface covered by ice floes, Phys. Fluids (ISSN: 10897666) 36 (3) (2024) http://dx.doi.org/10.1063/5.0200538.

[39] A.V. Slunyaev, Y.A. Stepanyants, Modulation property of flexural-gravity waves on a water surface covered by a compressed ice sheet, Phys. Fluids (ISSN: 10897666) 34 (7) (2022) http://dx.doi.org/10.1063/5.0100179.

[40] Raphael Stuhlmeier, Conor Heffernan, A. Alberello, Emilian Părău, Modulational instability of nonuniformly damped, broad-banded waves: applications to waves in sea ice, Phys. Rev. Fluids 9 (9) (2024) 094802, http://dx.doi.org/10.1098/rsta.2021.0255, URL https://link.aps.org/doi/10.1103/PhysRevFluids.9.094802.

[41] A.R. Osborne, Nonlinear Ocean Waves and the Inverse Scattering Transform, first ed., Elsevier, ISBN: 9780080925103, 2010.

[42] Amin Chabchoub, Miguel Onorato, Nail Akhmediev, Hydrodynamic Envelope Solitons and Breathers, Springer, 2016, pp. 55–87, http://dx.doi.org/10.1007/978-3-319-39214-1_3.